Laser guide star adaptive optics imaging polarimetry of Herbig Ae/Be stars

Marshall D. Perrin, James R. Graham, Paul Kalas, James P. Lloyd, Claire E. Max, et al.

Marshall D. Perrin, James R. Graham, Paul Kalas, James P. Lloyd, Claire E. Max, Donald T. Gavel, Deanna M. Pennington, Elinor L. Gates, "Laser guide star adaptive optics imaging polarimetry of Herbig Ae/Be stars," Proc. SPIE 5490, Advancements in Adaptive Optics, (25 October 2004); doi: 10.1117/12.551932

SPIE.

Event: SPIE Astronomical Telescopes + Instrumentation, 2004, Glasgow, United Kingdom

Laser Guide Star Adaptive Optics Imaging Polarimetry of Herbig Ae/Be Stars

Marshall D. Perrin[a,b], James R. Graham[a,b], Paul Kalas[a,b], James P. Lloyd[c,b], Claire E. Max[d,b], Donald Gavel[e,b], Deanna M. Pennington[d,b] Elinor L. Gates[f,b]

[a]UC Berkeley, 601 Campbell Hall, Berkeley CA 94720 [b]Center for Adaptive Optics, University of California, 1156 High Street, Santa Cruz CA 95064 [c]California Institute of Technology, 1201 East California Blvd, Pasadena CA 91125 [d]Lawrence Livermore National Laboratory, 7000 East Avenue, Livermore CA 94550 [b]Laboratory for Adaptive Optics, University of California, 1156 High Street, Santa Cruz CA 95064 [f]UCO/Lick Observatories. P.O. Box 85, Mount Hamilton, CA 95140

ABSTRACT

Current and future large telescopes depend critically on laser guide star adaptive optics (LGS AO) to achieve their scientific goals. However, there are still relatively few scientific results reported from existing LGS AO systems. We present some of the first science results from the Lick Observatory sodium beacon LGS AO system. We achieve high sensitivity to light scattered in the circumstellar enviroment of Herbig Ae/Be stars on scales of 100-200 AU by coupling the LGS AO system to a near-infrared (J, H, K_s bands) dual channel imaging polarimeter. We describe the design, implementation, and performance of this instrument. The dominant noise source near bright stars in AO images is a "seeing halo" of uncorrected speckles, and since these speckles are unpolarized, dual-channel polarimetry achieves a significant contrast gain. Our observations reveal a wide range of morphologies, including bipolar nebulosities with and without outflow-evacuated cavities and disk-mediated interaction among members of a binary. These data suggest that the evolutionary picture developed for the lower-mass T Tauri stars is also relevant to the Herbig Ae/Be stars, and demonstrate the ability of LGS AO systems to enhance the scientific capabilities of even modest sized telescopes.

Keywords: Laser guide stars, polarimetry, star formation

1. INTRODUCTION

Direct imaging of circumstellar disks and planetary companions requires both high angular resolution and high dynamic range. Dynamic range in adaptive optics (AO) observations is limited by speckle noise, which is substantially larger than photon noise near bright stars. A coronagraph can reduce speckle noise to a limited extent: The 'pinning' of speckles to bright diffraction rings in the typical point spread function (PSF) increases speckle noise, so to the extent that a coronagraph suppresses the PSF, it will reduce speckle noise.[1] However, unpinned speckles will still form a noisy halo around the star,[2] even in the case of an ideal coronagraph which achieves perfect suppression of the diffraction-limited portion of the wavefront. The fraction of starlight in this halo scales roughly as $1/(1-S)$ where S is the Strehl ratio. Space-based telescopes operating with near-unity Strehl ratios, such as the planned Terrestrial Planet Finder, may have negligible levels of speckle noise, but ground-based telescopes even with AO are currently limited to Strehl ratios < 0.7 in the near-IR, making speckle noise a significant problem in high dynamic range imaging. The use of differential imaging techniques, either dual-channel polarimetry or multi-wavelength imaging, is required to suppress speckle noise and achieve the highest dynamic range.

Differential polarimetry is a powerful tool for overcoming speckle noise. As atmospheric speckles are not themselves polarized for scattering angles less than a few arcseconds, the differencing of simultaneous images taken in perpendicular polarizations will remove the unpolarized speckles. This provides an increase in contrast for light which has been polarized by scattering from circumstellar material. This technique has been used to

mperrin@astro.berkeley.edu; 1 510 642 1916; fax 1 510 642 3411; astron.berkeley.edu/ mperrin/

Advancements in Adaptive Optics, edited by Domenico Bonaccini Calia, Brent L. Ellerbroek, Roberto Ragazzoni, Proceedings of SPIE Vol. 5490 (SPIE, Bellingham, WA, 2004)
0277-786X/04/$15 · doi: 10.1117/12.551932

obtain images of circumstellar disks around several stars, including HD 169142,[3] GG Tau and GM Aur,[4] and TW Hya.[5] All of these detections have been around relatively bright, nearby YSOs, through the use of natural guide star (NGS) AO. However, a magnitude-limited NGS survey may be biased by the fact that young stellar objects (YSOs) are generally found in regions of high extinction. Particularly for the youngest YSOs or for systems with an edge-on orientation, extinction may result in V magnitudes too dim for NGS AO. Laser guide star (LGS) AO is therefore important as a complement to NGS AO for studies of the complete range of YSO properties.

The Lick/Lawrence Livermore National Laboratory adaptive optics system (henceforth, "Lick AO") was developed by UC and LLNL staff and has been in operation on the Lick 3-m Shane telescope since the mid 1990s,[6] including in recent years a laser guide star (LGS) capability.[7] The wavefront sensor is a 40-subaperture Shack-Hartmann design while the deformable mirror has 61 degrees of freedom inside the telescope aperture. In conjunction with the science camera IRCAL,[8] it routinely achieves internal Strehl ratios $S > 0.9$, and on-the-sky Strehl ratios up to 0.7 at 2.1 μm, corresponding to an RMS wavefront error of 200 nm.

In LGS mode, the atmospheric wavefront reference is created by a laser tuned to the sodium D2 line at 589 nm, which excites mesospheric sodium at roughly 90 km altitude. The 589 nm light is generated by a tunable dye laser pumped by a set of frequency-doubled solid-state (Nd:YAG) lasers. Typically, 11-14 W of average laser power is projected into the sky with a pulse width of 150 ns and a pulse repetition rate of 13 kHz. The laser is launched from a 30 cm refractive telescope mounted on the side of the 3 m (Figure 2).

Achievable Strehl ratios in LGS mode are generally less than in NGS mode, $S < 0.4$, and may be < 0.2 in poor seeing conditions. As a result, LGS observations currently suffer more from PSF variability and have a greater fraction of light in the speckle halo than NGS observations. Differential polarimetry is a particularly useful tool in such circumstances since it tends to minimize the detrimental effects of the speckle halo.

2. METHODS

The IRCAL science camera uses a 256^2 pixel HgCdTe PICNIC array manufactured by Rockwell. The plate scale of 0.0754 $''$pixel^{-1} Nyquist-samples a diffraction-limited at K_s band (2.1 microns) and provides a field of view $\sim 19.4''$ on a side. While IRCAL was not originally designed with a polarimetry mode, a relatively straightforward upgrade was able to add this capability through a YLF Wollaston prism and rotating half-wave plate.

2.1. Wollaston Prism

A Wollaston prism placed in a collimated beam will slightly deviate perpendicular polarizations, forming on the detector two simultaneous images from the ordinary and extraordinary rays. A polarization modulator is required in order to measure both Stokes Q and U. As described in,[3] further modulations which swap polarization states between the two sides of the detector can be used to minimize the effects of flat fielding or other systematic errors.

While the most traditional material for Wollaston prisms is calcite, a number of other materials have been discussed[9] and in some cases used. In particular, calcite becomes opaque to the ordinary beam at 2.2 microns, and so for K-band polarimetry we are forced to turn to alternative materials.

We chose YLF (Yttrium Lithium Floride, pronounced "yilf" by its users in the laser industry) for our prism for several reasons. Its refractive index, 1.45, is comparable to that of standard optical components and cements, thus simplifying the optical design and manufacturing. The difference in index of refraction between polarizations, $\Delta n = 0.022$, allows the necessary beam divergence to be obtained with an easily achievable thickness of YLF, roughly 4 mm.

Most importantly, Δn is remarkably constant with wavelength, allowing broad-band imaging in all near-IR bands with minimal chromatic elongation: Any change of Δn with wavelength will result in different beam displacement for each wavelength within a bandpass, elongating the final image in that direction and reducing the ultimate resolution of the system. This lateral chromatism effect may be quantified over a wavelength range $\lambda_1 < \lambda < \lambda_2$ by Oliva's parameter $V = \frac{\Delta n_{(\lambda_1+\lambda_2)/2}}{\Delta n_{\lambda_1} - \Delta n_{\lambda_2}}$ which gives the image elongation ϵ over the range $\lambda_1 - \lambda_2$ as

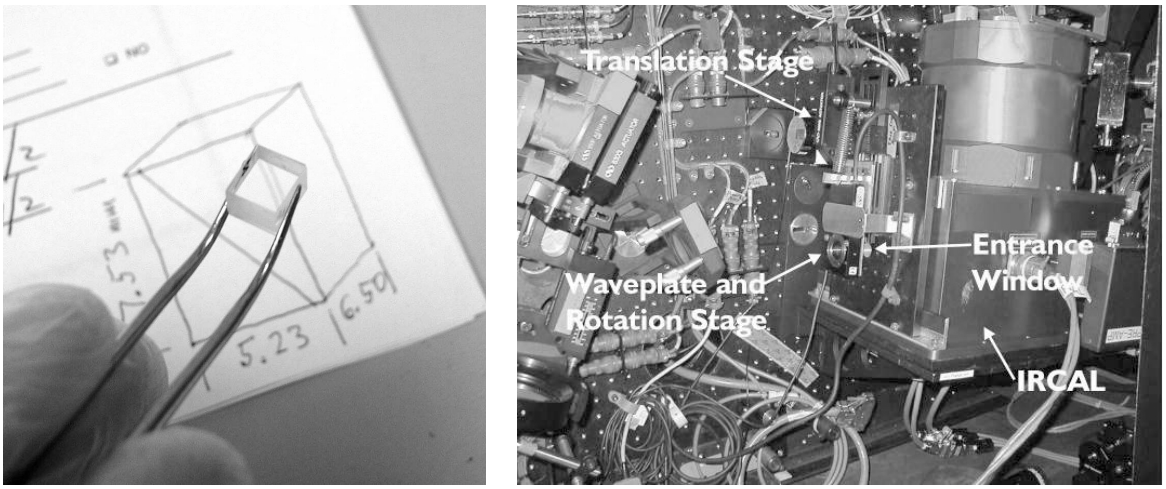

Figure 1. Left: Our YLF Wollaston prism prior to installation in the IRCAL dewar. Note how the prism visibly splits the line from the diagram in the background. **Right:** The IRCAL dewar mounted on the Lick AO optical bench, with the waveplate mechanisms labeled.

$\epsilon = \delta/V$. Therefore by selecting a material to maximize V, we can minimize the effects of lateral chromatism. Typically, $V > 100$ is considered good, corresponding to chromatic elongation less than $0.05''$for IRCAL, better than the diffraction limit. YLF exceeds this for all NIR bandpasses (spectacularly at H, with $V = 1290$), along with $AgGaS_2$ and CdSe, but YLF is most readily available at reasonable cost due to its widespread use in the laser industry. Our desire to not compromise the resolving power of the system led us to choose YLF for our Wollaston prism.

Three similar Wollaston prisms were fabricated by Onyx Optics of Dublin, CA and were received at Berkeley in March 2002. The final prism dimensions were 5 mm$\times$6 mm$\times$7 mm, with a 30 degree prism angle. The pieces were joined using optical contacting and both exterior surfaces received a 1-2.5 micron antireflection coating. All three prisms performed as expected in laboratory tests with polarized 650 nm light, with beam divergences between 1.49 and 1.55 degrees. Two of the prisms exhibited minor surface defects from the manufacturing process; the third prism was chosen for astronomical use and installed into one of IRCAL's filter wheels. To prevent overlap of the two polarized images, an aperture mask corresponding to half the field of view was fabricated and installed in IRCAL's cold aperture mask wheel.

2.2. Polarization modulator

Polarization modulation may be accomplished either through the use of a rotating half-wave plate or with liquid crystal variable retarders (LCVRs). Each of these approaches has certain advantages and disadvantages: In addition to rotating the polarization states, a pair of LCVRs can also convert circular to linear polarization allowing measurement of Stokes V. Furthermore, the lack of any moving optical elements eliminates the image wander and flat field variations which can occur with rotating wave plates. However, LCVRs are generally not achromatic, are difficult to obtain for wavelengths beyond 1.8 microns, and have birefringence which is temperature-dependent. In contrast, half-wave plates are available with excellent achromaticity and low sensitivity to temperature variations. Since we desired a single polarization modulator for the entire 1-2.5 micron band, we chose to use an achromatic waveplate rather than LCVRs.

It was decided to mount the waveplate at the entrance window to IRCAL; a cold waveplate would have been preferable, but posed too severe engineering difficulties given limited space inside the dewar. An achromatic waveplate optimized for 1-1.6 microns was obtained from Karl Lambrecht Corp. and mounted in a Newport PR50 rotation stage. This was itself mounted on a translation stage attached to the IRCAL dewar adjacent to the entrance window to allow insertion into the beam. The rotation and translation drives were connected to formerly spare channels on the Lick AO system motor controller and integrated into the AO controller software.

The flexibility of the Lick AO software architecture made it easy to integrate the waveplate controls into the existing AO operator console. Furthermore, the Tcl/Tk-based software interface between the IRCAL and AO user interfaces[8] allows control of the waveplate from the IRCAL GUI, enabling scripts to automate polarimetry observations.

2.3. Data Reduction

Observation with our polarimeter is straightforward, with most of the complications relegated to the data reduction pipeline. Once the target has been acquired by the telescope and AO system, the observer configures exposure parameters such as filter and exposure time. A polarimetry script automatically rotates the waveplate and integrates at each position. We have chosen to use eight distinct waveplate positions: 0, 22.5, 45, 67.5, 90, 112.5, 135, and 157 degrees. This provides four redundant measurements for each of Stokes Q and U. Typically exposure durations are 5-90 s, depending on source magnitude. Small dithers of a few arcseconds after each set of eight exposures are used to minimize flat field effects and increase field of view. We also obtain sky frames using identical procedures on nearby regions devoid of sources (usually 30-90″away from the science target). Flat fields are obtained from exposures on the twilight sky with the polarimetry optics in place, while dark frames are obtained at the end of the night using the usual IRCAL procedures.

The polarized images are combined using a double differencing approach[3] which provides increased robustness against flat-fielding errors. The many off-axis reflections in the AO system and camera optics are expected to introduce an instrumental polarization bias. We have tried two different approaches for removing this bias. Unpolarized standard stars have been observed to determine the instrumental bias. A bias of $p \sim 2\%, \theta = 85°$ has been found, with the exact magnitude varying slightly with wavelength. We believe the greatest contribution to this bias comes from the dichroic beamsplitter in the AO system. The measured bias is then subtracted through Mueller matrix operations on the data.[10]

Alternatively, when differencing the polarized images, a multiplicative scale factor may be included to minimize the total residual intensity in the difference image. Essentially, the star itself is assumed to be intrinsically unpolarized and we are solving for its apparent polarization due to instrumental effects. This approach has the benefit of also implicitly removing any interstellar polarization, but there is greater uncertainty in the derived polarization values due to the assumptions involved. This latter approach is most appropriate when searching for spatially-varying polarization signals, such as the centrosymmetric signature of a circumstellar disk, while the former approach is better if absolut polarization calibration is imporant.

Both algorithms result in a final difference image for each of Stokes Q and U, while the sum of all observations provides Stokes I. It is also frequently useful to display the polarized intensity $P = \sqrt{(Q^2 + U^2)}$, which has the same dimensions as intensity I, or the fractional polarization $p = P/I$.

2.4. Performance

The prism was installed into the IRCAL filter wheel during March 2002, and had first astronomical light on the night of 28 March 2002. Observations that night and on subsequent nights, as well as engineering test observations carried out on calibration sources during the day, have allowed us to quantify the performance of the system.

With the waveplate and prism retracted, the Lick AO system and IRCAL typically achieve an internal Strehl ratio of slightly greater than 0.9 when observing the internal calibration source at 2.16 μm. (Strehl ratios are measured using the IRCAL quicklook software's Strehl tool.) The insertion of the waveplate into the converging beam introduces additional focal path length into the system, which was experimentally found to be 1.3 mm (consistent with its thickness and index of refraction). The prism appears to be somewhat astigmatic, and by applying appropriate modes to the deformable mirror to counter this astigmatism, the internal Strehl ratio was increased to $0.91 \pm .01$, essentially identical to the Strehl prior to the addition of the polarimeter optics. The magnitude of the image sharpening correction was not appreciably larger than corrections typically applied for semi-static non-common-path aberrations. Thus optical errors in the waveplate and prism do not appear to appreciably degrade image quality.

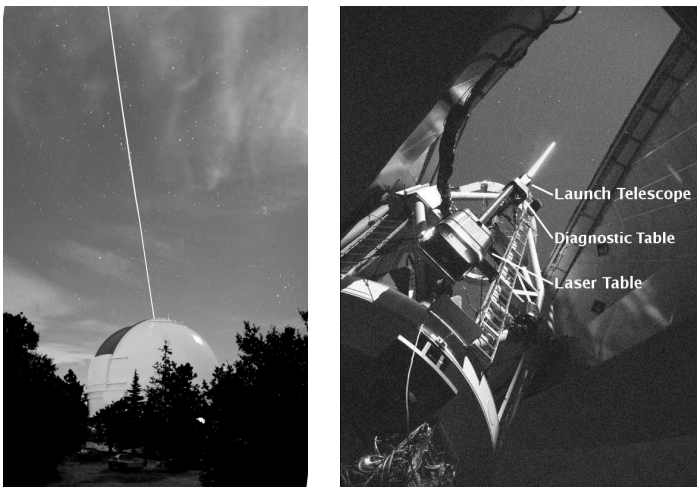

Figure 2. Left: The Lick Observatory 3-m with the LGS system in operation. This photograph was taken during the observations of LkHα 225 presented in this paper. **Right:** The 3-m Shane telescope with components of the LGS system marked. The pump lasers are located in a room below the dome floor and are fiber-optically coupled to the dye laser in the laser table. Photo courtesy of David Whysong.

In an ideal case, the two polarization images for an unpolarized source would have precisely identical point spread functions and would subtract down to the photon noise level in the difference image. In reality, non-common path effects will lead to different wavefronts in the two channels, degrading system performance. In our case there remain noticable differences in the point spread functions of the ordinary and extraordinary rays. Even after careful attention to flat-fielding, subpixel alignment of the two images, and removal of instrumental polarization, subtraction residuals are generally $\approx 0.5 - 1.0\%$ of the total intensity. This crosstalk between the total intensity and polarized intensity signals provides the dominant limit on sensitivity very close to stars.

The source of this crosstalk is still under investigation, with two leading hypotheses remaining. The first is that there may still be residual errors in the subpixel centering of the images. This task is particularly difficult for IRCAL as the detector does not Nyquist sample the diffraction limit at J or H band. Secondly, the IRCAL camera geometry is such that the two filter wheels are located prior to the cold stop which defines the system pupil. Since the Wollaston prism changes the angle of the two polarized beams in collimated space, the two beams will diverge slightly before encountering the cold pupil and thus the effective system pupil will differ for the two channels. In both cases, the crosstalk could be reduced by stopping down the beam before the Wollaston prism, at the cost of slightly degraded angular resolution and light-gathering power. This will be tested on future observing runs.

The effect of the crosstalk is to limit our sensitivity to scattered light which is $\gtrsim 2\%$ polarized. Light scattered by circumstellar dust is often several tens of percent polarized, so we have continued with observations while still working on improving polarimeter performance. Nonetheless, this issue could have been easily avoided had implementation of a polarimetric mode been considered during the initial science camera design. This lesson is particularly relevant to the current design efforts for "Extreme AO" direct planet-imaging instruments: optimizations for polarimetric performance should be considered in trade studies early in the design process of both AO systems and science instruments.

3. OBSERVATIONS OF HERBIG AE/BE STARS

Herbig Ae/Be stars are young stars with masses between 1.5 and 10 times that of the sun; they are the intermediate-mass counterparts of the more common T Tauri stars. Excess infrared and millimeter emission shows that Herbig Ae/Be stars are associated with abundant circumstellar dust.[11]

Table 1. Observation Log

Object	V	Distance (parsec)	SpTyp	Luminosity ($L_\odot$)	Mass ($M_\odot$)	Date Obs. (UT)	Bands	Time per band (s)
LkHα 225	15.2-18	980		1600		2003-07-22	J, H, K_s	960
LkHα 198	14.3	600	A5e-A7e	5.6	1.2	2003-07-23	J, H, K_s	960
LkHα 233	13.6	880	A5e	28.2	2.6	2003-07-23	J, H, K_s	1440
VY Mon	13.7-17.4	900	O9-F2?			2003-11-18	H	480

Table 2. Observation log and target properties, where known. V magnitude, distance, luminosity, and mass are from[11] for LkHα 198 and 233, from[15] and[16] for LkHα 225, and from[15] and[17] for VY Mon.

Observations of T Tauri stars have led to a general understanding of the origin of solar-type stars[12] as a process of accretion mediated by angular momentum transfer in circumstellar disks, giving rise to bipolar outflows. It has been hypothesized that the more massive Herbig Ae/Be stars and the T Tauri stars form and evolve in similar manners,[13] but this remains controversial. It has been suggested that even higher-mass star formation may require additional mechanisms, such as stellar mergers, to overcome the radiation pressure that would otherwise terminate accretion. The Herbig Ae/Be stars form an intermediate class of objects where such effects may or may not be relevant. Hα spectropolarimetry reveals different line polarization effects between the Herbig Ae and Herbig Be stars,[14] suggesting there may be a transition in the physical characteristics between these classes as presumably the mode of accretion changes. Spatially resolved images of these objects may help clarify this.

Laser guide star observations of several Herbig Ae/Be stars were obtained with the polarimeter in July and November 2003. Natural guide star observations have also been obtained and will be discussed in a future work. An observation log is presented in table 2. Laser guide star systems are insensitive to tip and tilt, requiring a separate tip/tilt sensor using a natural guide star. For the observations presented here, the science targets served as their own tip/tilt references.

3.1. LkHα 198 and LkHα 233

Our observations of the Herbig Ae/Be stars LkHα 198 and LkHα 233 have previously been reported[18] and we present here only a summary of the science results. The atmospheric seeing was good ($0.8''$at 550 nm), but the mesospheric sodium density was low. This decreased the magnitude of the guide star, forcing the adaptive optics system to operate at its lowest frame rate of 55 Hz. As a result, the Strehl ratios achieved were modest ($S \approx 0.05 - 0.1$) despite the good atmospheric seeing. Correspondingly, the full-width at half-maximum (FWHM) of the point spread function was larger than the FWHM of a diffraction limited beam, $0.27''$versus $0.15''$respectively at 2.1 microns.

LkHα 198 and LkHα 233 are both classified as Hillenbrand Group II Herbig Ae/Be stars: they have infrared spectra that are flat or rising towards longer wavelengths. This means that they are young stars that may or may not possess circumstellar disks but do possess circumstellar envelopes which are not confined to a disk plane. We observe such envelopes around both of our sources in the form of centrosymmetrically polarized biconical nebulosities viewed approximately edge-on to the midplanes.

LkHα 198 is located at the head of an elliptical loop of optical nebulosity extending 40 arcseconds to the star's southeast.[19] We discover a biconical nebula $\sim$10 arcseconds in diameter (6000 AU), oriented north-south, with polarization vectors concentric with respect to LkHα 198 (Fig. 3). The lobes of the reflection nebula are divided by a dark, unpolarized lane that we interpret as a density gradient towards the equatorial plane of a circumstellar disk and/or a flattened envelope. The deep exposures needed to observe this nebulosity resulted in saturation in the inner core of the PSF so we cannot measure colors for LkHα 198. Nonetheless, the fact that we see a bright source in an apparently edge-on geometry indicates low extinction inconsistent with a dense disk. Unsaturated observations will be obtained in a future observing run to investigate this further.

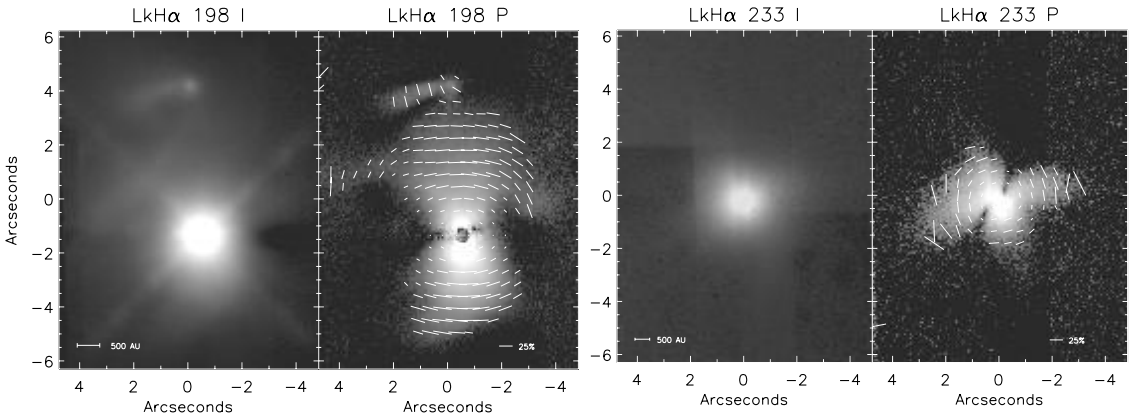

Figure 3. Left: H band polarized intensity for LkHα 198. Vectors show magnitude and position angle of polarization. **Right:** The same but for LkHα 233. All images are shown using logarithmic stretches.

The embedded source LkHα 198-IR[20] is detected in our H and K_s band data 5.5″ from LkHα 198 at PA=5°. A polarized, extremely blue, jet-like feature extends $> 2''$ (1200 AU) from LkHα 198-IR at PA=105°.[21] The polarization vectors of this apparent jet are perpendicular to its long axis, indicating that LkHα 198-IR is the illuminating source, not LkHα 198. The orientations of circumstellar structures revealed by our images confirm that LkHα 198-IR is the best candidate for the origin of the Herbig-Haro outflow to PA 135°. By extension, the large elliptical nebula to the southeast was most likely created by outflow from LkHα 198-IR, although we see it primarily in scattered light from the optically much brighter LkHα 198.

LkHα 233 is an embedded A5e-A7e Herbig Ae/Be star which is associated with a blue, rectangular reflection nebula 50″in extent, located in the Lac OB1 molecular cloud at 880 parsecs. Our imaging polarimetry reveals four distinct lobes bisected by a narrow, unpolarized lane with PA$\approx$ 150° (Fig. 3). The east-west extent of this nebulosity decreases from 6″(5300 AU) at J and H to 2″(1800 AU) at K_s. The orientation of the lobes relative to the dark lane suggests that they are the limb-brightened edges of a conical cavity in a dusty envelope illuminated by a highly extincted star. The radial extent of the dark lane (1000 AU) suggests that it is associated with an equatorial torus characteristic of a flattened infalling protostellar cloud,[22] and not a rotationally-supported disk. We find that the intensity peak of the star is shifted southwest relative to the polarization centroid, with the displacement increasing from 0.15″at K_s to 0.35″at J. We do not see the star directly, but instead view a scattering surface above the disk midplane.

LkHα 233's limb-brightened appearance provides compelling evidence for the presence of cavities swept out by bipolar outflow from the star. Cavity models with an opening angle of 30-40° seen at an inclination of 80° reproduce both the observed polarization fraction of 25-40% and the higher degree of limb brightening seen in the near lobe. The absence of limb brightening may be evidence that LkHα 198 lacks polar cavities, or possesses ones which are either very narrow or which have a higher average dust density.[18]

Based on these observations, LkHα 233 appears to be the more evolved of the two systems, with well-defined cavities swept out by bipolar outflow and bisected by a very dark lane. LkHα 198 is a less evolved system, which is only in the early stages of developing bipolar cavities and possesses lower extinction in the apparent disk midplane. The observed circumstellar environments of these Herbig Ae stars are consistent with the rotationally-flattened infall envelopes models developed for T Tauri stars,[23] indicating that the process of envelope collapse has similar phases, despite the large disparities in mass and luminosity between these two classes of young stars. This morphological similarity leads us to infer that the conservation and transport of angular momentum is the dominant physical process for both classes of stars.

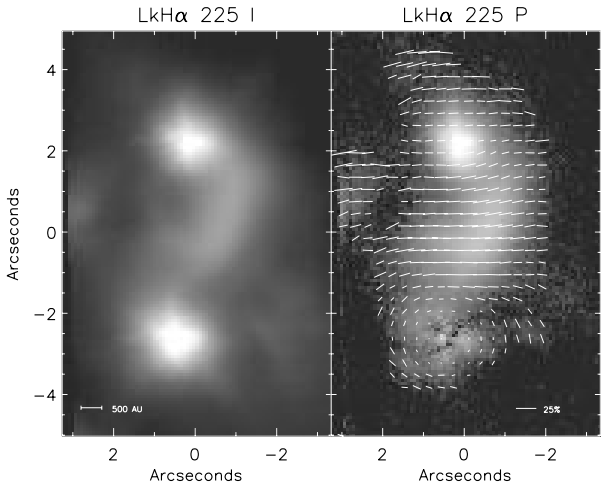

Figure 4. H band total intensity and polarized intensity for LkHα 225. Vectors show magnitude and position angle of polarization.

3.2. LkHα 225

LkHα 225 (V 1318 Cyg) is an apparent binary located in a cluster which also includes the Herbig AE/Be stars BD +40°4124 and LkHα 224. It has been proposed that LkHα 225 consists of a young, low-mass star, LkHα 225N, and an intermediate-mass, very young Herbig Ae/Be star, LkHα 225S, based on luminosity arguments.[24] The two stars have JHK colors and K-band spectra typical of class YSOs, with an additional component of emission coming from a more extended envelope; the extinction to the stars is $A_V \sim 10$ mag.[25]

Our observations of LkHα 225 encountered two technical difficulties. A temporary communications problem between the AO system and telescope impaired tip-tilt offloading, resulting in somewhat increased image motion. Secondly, as the star passed near zenith (4° at transit), the slant path to the sodium layer became less than the minimum focal distance of the wavefront sensor. The AO system was still able to lock on the slightly defocused laser spot, but the quality of correction suffered. The focus travel has since been increased to resolve this limitation. Estimating the achieved Strehl ratio is complicated by the tail of emission between the two stars, but roughly $S \sim 0.1$.

A comma-shaped reflection nebula extends from LkHα 225N towards LkHα 225S.[25] This appears as the bright filament evident in our imaging polarimetry. We discover a fainter bar extending west from LkHα 225S. In these new observations a continuous streamer can be traced from the NW of LkHα 225N, though LkHα 225S and terminating 2″ west of LkHα 225S. A disconnected region of scattered light appears about 4″ NE of LkHα 225S; the polarization position angle indicates that this is illuminated by LkHα 225S. We measure at H band the binary position angle of LkHα 225 to be 356° and the separation 4.9″, or about 4800 AU at the distance of the cluster (980 pc;[16]). We also detect three nearby faint point sources, with $\Delta H = 4.9, 4.9, 5.5$; $\rho = 10.8'', 3.3'', 3.5''$ and PA= 350°, 140°, 130° respectively relative to 225S.

The orientation of the polarization vectors confirms that both LkHα 225N and 225S illuminate the filament: the vectors are centered on 225N at the north end of the filament, changing smoothly to the south to become centered around 225S. These objects are thus physically associated rather than just being a chance line-of-sight alignment. The polarization is highest on the inner side of the curved filament, facing towards 225N; the outer side may be less polarized due to higher optical depth resulting in multiple scattering, or because illumination from both 225S and 225N arrives from different position angles. Likewise, there is an indication that LkHα 225N has a faint bar to its north.

The filament may be a remnant from the collapse of the cloud core from which the stars formed, may be associated with the outflow from LkHα 225S, or as the morphology suggests, may be material tidally stripped

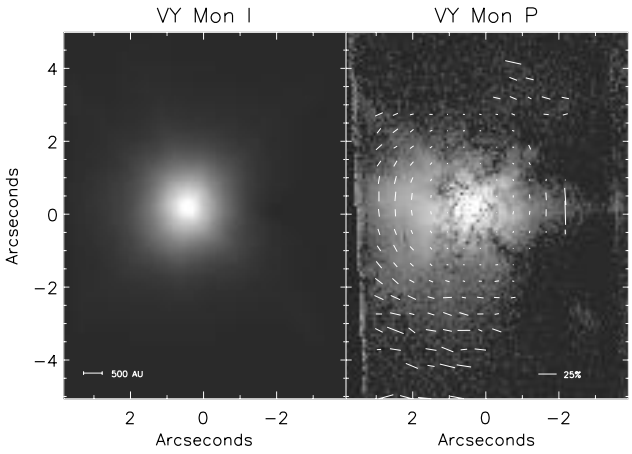

Figure 5. *H* band total and polarized intensity for VY Mon. Vectors show magnitude and position angle of polarization. The vertical line at left in the polarized intensity image is an artifact from the edge of the field of view.

from the circumstellar environments of LkHα 225 N and S in a close encounter. It has been proposed that drag caused by gravitational star-disc interactions could be an important binary formation mechanism.[26] For the most common encounters, in which the periastron distance is much greater than the disc radius, energy and angular momentum are in general transferred from the disc to the stars.[27] Thus long-range encounters do not provide a mechanism for capture. Further observations and modelling of this system will be necessary to estimate periastron passage. The putative tidal streamers in the field of LkHα 225 are resolved into clumps. Weak interactions can trigger fragmentation of the disc, via tidally and compressionally induced gravitational instabilities, leading to the formation of additional stars and substellar objects.[28]

We have explored the parameter space for dynamical models that have one star with a circumstellar disk experience a single, close, parabolic encounter by a star without a disk. The general result is that the star without a disk captures some material, both stars have a one-arm spiral structure, and these arms are connected to each other by a tenuous bridge of material. The star that originally had the circumstellar disk has the strongest counterarm. Since the brightest part of the tail extends southeast from 225N, if that material was stripped from a disk around 225N, that disk must be rotating counterclockwise in the plane of the sky. On the other hand, the millimeter continuum data support a picture where LkHα 225S is surrounded by a more massive circumstellar disk than 225N, which makes it puzzling that brighter tail is closer to 225N. Velocity information would help to constrain models. Unlike LkHα 198 and 233 there is no clear evidence for a biconical reflection nebula or occulting disk around either member of LkHα 225. However, while LkHα 225S has centrosymmetric polarization vectors around a region of low polarization at the position of the star, LkHα 225N displays $\gtrsim 10\%$ polarization oriented east-west. This difference in morphology suggests that circumstellar disks around these two stars, if present, are likely not coplanar.

The T Tauri system SR 24 also shows a bridge of material extending from SR 24 S to SR 24 Nab. As with LkHα 225, polarimetric observations have confirmed that this material is physically assocated with the stars.[29] Comparative studies of these two objects may further illuminate the role of collisional encounters in both low and intermediate mass star formation.

3.3. VY Mon

VY Mon is an Algol-like variable star in the Monoceros OB1 association ~ 900 pc distant. Its spectral type is uncertain: the literature includes estimates of O9,[30] B8,[31] A5,[32] and F2.[17] It has been previously reported to be slightly extended to the south in K-band imaging, and is coincident with the core of a $\sim 2'$ extended millimeter source.[33] VY Mon is the brightest mid-IR to submillimeter source in this region, appearing as a

bright point source from 12-370 μm.[34] Its flat SED makes it a Hillenbrand Group II object, like LkHα 198 and LkHα 233.

The V magnitude of VY Mon varies between 13.7-17.4.[15] Based on wavefront sensor counts it was approximately $V \approx 15$ when we observed it in November 2003 in poor seeing conditions. AO correction was minimal: Strehl ratio ≈ 0.03, FWHM $= 0.5''$. Nonetheless, we detect centrosymmetrically polarized light surrounding VY Mon in H band, indicative of dust scattering in an extended envelope. The polarized light forms a roughly elliptical region, $6''$east-west and $3''$north-south. This region is not centered on the star: the polarization is stronger to the south and east than in the opposite directions. A peak polarization of 13% is observed $2''$east of the star, though we caution this is likely an underestimate of the intrinsic polarization due to contamination by uncorrected starlight. Our field of view does not include either of the companions imaged at 10 microns,[35] but we do detect a $\Delta H = 6.2 \pm 1$ companion at $\rho = 9''$, PA $= 332°$.

Further observations with better resolution and at additional wavelengths are necessary to constrain the properties of VY Mon.

4. CONCLUSIONS

Laser guide star system have matured to the point of producing useful scientific data. However, in our experience, achievable Strehl ratios remain lower than those obtainable through NGS AO. This is due in part to LGS systems' susceptibility to performance loss due to adverse atmospheric conditions of both poor seeing and low atmospheric sodium density.

However, we have demonstrated that useful observations may be obtained with LGS systems even in such non-ideal conditions. This is particularly true when simultaneous differential imaging techniques such as dual-channel polarimetry are used to reduce the effects of speckle noise and PSF variability. As LGS AO systems come into maturity on the 8-10 meter telescopes, differential techniques are likely to remain useful for maximizing the science return.

Even though AO systems involve large numbers of optics and many off-axis reflections, properties generally considered undesirable for precision polarimetry, AO polarimetry is in fact capable of sensitively probing the circumstellar environments of stars. The instrumental polarization bias at Lick is extremely stable with time, changing $< 0.1\%$ in observations of standard stars more than a year apart. The fact that the Lick AO system is a Cassegrain instrument helps here by keeping the AO system and telescope fixed relative to one another. However, the changing geometry of Nasmyth and Coude foci does not preclude polarimetry: the dominant instrumental bias is expected to come from the AO system, which is fixed relative to the science camera. Furthermore, if the science drivers require only differential imaging polarimetry across a spatially resolved target, then knowing the absolute polarization bias to a high degree of precision is not needed. In that case data reduction techniques which implicitly solve for the instrumental polarization during the reduction process may be used. Imaging polarimetry has recently been demonstrated with NACO[5] at the Nasmyth focus of VLT UT4, and in the coming year a polarimetry upgrade to the Lyot Project AEOS Coronagraph[36] will demonstrate polarimetry with a Coude AO system. Future LGS AO operations on the VLT and Keck telescopes are likely to include polarimetry observations as well.

ACKNOWLEDGMENTS

We are indebted to the Lick Observatory staff who assisted in these observations, including Tony Misch, Kostas Chloros, and John Morey, and also to the many individuals who have contributed to making the laser guide star system a reality. Onyx Optics in Dublin, California fabricated our YLF Wollaston prisms. This work has been supported in part by the National Science Foundation Science and Technology Center for Adaptive Optics, managed by the University of California at Santa Cruz under cooperative agreement No. AST-9876783; and also under the auspices of the U.S. Department of Energy, National Nuclear Security Administration by the University of California, Lawrence Livermore National Laboratory under contract No. W-7405-Eng-48. PK received additional support from the NASA Origins Program under grant NAG5-11769. MDP is supported by a NASA Michelson Graduate Fellowship, under contract to the Jet Propulsion Laboratory (JPL). JPL is managed for NASA by the California Institute of Technology.

REFERENCES

1. R. Soummer and C. Aime, "Usefulness and limits of coronagraphy in the presence of pinned speckles," *Astrophys. J. Lett.* **0**, p. Submitted, 0 2004.
2. M. D. Perrin, A. Sivaramakrishnan, R. B. Makidon, B. R. Oppenheimer, and J. R. Graham, "The Structure of High Strehl Ratio Point-Spread Functions," ApJ **596**, pp. 702–712, Oct. 2003.
3. J. R. Kuhn, D. Potter, and B. Parise, "Imaging Polarimetric Observations of a New Circumstellar Disk System," ApJ **553**, pp. L189–LL191, June 2001.
4. D. E. Potter, "A search for debris disks with a dual channel adaptive optics imaging polarimeter," *Ph.D. Thesis* , Nov. 2003.
5. D. Apai, I. Pascucci, W. Brandner, T. Henning, R. Lenzen, D. E. Potter, A.-M. Lagrange, and G. Rousset, "NACO polarimetric differential imaging of TW Hya. A sharp look at the closest T Tauri disk," A&A **415**, pp. 671–676, Feb. 2004.
6. C. Max, S. Olivier, H. Friedman, J. An, K. Avicola, B. Beeman, H. Bissinger, J. Brase, G. Erbert, D. Gavel, K. Kanz, M. Liu, B. Macintosh, K. Neeb, J. Patience, and K. Waltjen, "Image improvement from a sodium-layer laser guide star adaptive optics system," *Science* **277**, pp. 1649–1652, Sept. 1997.
7. B. J. Bauman, D. T. Gavel, K. E. Waltjen, G. J. Freeze, R. L. Hurd, E. L. Gates, C. E. Max, S. S. Olivier, and D. M. Pennington, "Update on optical design of adaptive optics system at Lick Observatory," in *Proc. SPIE Vol. 4494, p. 19-29, Adaptive Optics Systems and Technology II, Robert K. Tyson; Domenico Bonaccini; Michael C. Roggemann; Eds.*, **4494**, pp. 19–29, Feb. 2002.
8. J. P. Lloyd, M. C. Liu, B. A. Macintosh, S. A. Severson, W. T. Deich, and J. R. Graham, "IRCAL: the infrared camera for adaptive optics at Lick Observatory," in *Proc. SPIE Vol. 4008, p. 814-821, Optical and IR Telescope Instrumentation and Detectors, Masanori Iye; Alan F. Moorwood; Eds.*, **4008**, pp. 814–821, Aug. 2000.
9. E. Oliva, S. Gennari, L. Vanzi, A. Caruso, and M. Ciofini, "Optical materials for near infrared Wollaston prisms," A&AS **123**, pp. 179–182, May 1997.
10. R. W. Goodrich, "V645 Cygni and the duck nebula," ApJ **311**, pp. 882–894, Dec. 1986.
11. L. A. Hillenbrand, S. E. Strom, F. J. Vrba, and J. Keene, "Herbig Ae/Be stars - Intermediate-mass stars surrounded by massive circumstellar accretion disks," *Astrophys. J.* **397**, pp. 613–643, Oct. 1992.
12. F. H. Shu, F. C. Adams, and S. Lizano, "Star formation in molecular clouds - Observation and theory," *Ann. Rev. Astron. Astrophys.* **25**, pp. 23–81, 1987.
13. F. Palla and S. W. Stahler, "The Pre-Main-Sequence Evolution of Intermediate-Mass Stars," *Astron. J.* **418**, pp. 414–+, Nov. 1993.
14. J. S. Vink, J. E. Drew, T. J. Harries, and R. D. Oudmaijer, "Probing the circumstellar structure of Herbig Ae/Be stars," MNRAS **337**, pp. 356–368, Nov. 2002.
15. P. N. Kholopov, N. N. Samus, M. S. Frolov, V. P. Goranskij, N. A. Gorynya, E. A. Karitskaya, E. V. Kazarovets, N. N. Kireeva, N. P. Kukarkina, N. E. Kurochkin, G. I. Medvedeva, E. N. Pastukhova, N. B. Perova, A. S. Rastorguev, and S. Y. Shugarov, "Combined General Catalogue of Variable Stars (Kholopov+ 1998)," *VizieR Online Data Catalog* **2214**, pp. 0–+, Apr. 1999.
16. L. A. Hillenbrand, M. R. Meyer, S. E. Strom, and M. F. Skrutskie, "Isolated star-forming regions containing Herbig Ae/Be stars. 1: The young stellar aggregate associated with BD +40deg 4124," *Astron. J.* **109**, pp. 280–297, Jan. 1995.
17. J. Hernández, N. Calvet, C. Briceño, L. Hartmann, and P. Berlind, "Spectral Analysis and Classification of Herbig Ae/Be Stars," AJ **127**, pp. 1682–1701, Mar. 2004.
18. M. D. Perrin, J. R. Graham, P. Kalas, J. P. Lloyd, C. E. Max, D. T. Gavel, D. M. Pennington, and E. L. Gates, "Laser Guide Star Adaptive Optics Imaging Polarimetry of Herbig Ae/Be Stars," *Science* **303**, pp. 1345–1348, Feb. 2004.
19. W. Li, N. J. Evans, P. M. Harvey, and C. Colome, "Near-infrared (J, H, K) imaging of Herbig Ae/Be stars," *Astrophys. J.* **433**, pp. 199–215, Sept. 1994.
20. P. O. Lagage, G. Olofsson, S. Cabrit, C. J. Cesarsky, L. Nordh, and J. M. Rodriguez Espinosa, "A Deeply Embedded Companion to LkH alpha 198," *Astrophys. J. Lett.* **417**, pp. L79+, Nov. 1993.

21. M. Fukagawa, M. Tamura, H. Suto, Y. Itoh, K. Murakawa, Y. Oasa, S. S. Hayashi, T. Naoi, N. Kaifu, and Y. Doi, "Subaru Near-IR Coronagraphic Image of LkHα 198," *Pub. Astron. Soc. Japan* **54**, pp. 969–973, Dec. 2002.
22. S. Terebey, F. H. Shu, and P. Cassen, "The collapse of the cores of slowly rotating isothermal clouds," *Astrophys. J.* **286**, pp. 529–551, Nov. 1984.
23. B. A. Whitney, K. Wood, J. E. Bjorkman, and M. Cohen, "Two-dimensional Radiative Transfer in Protostellar Envelopes. II. An Evolutionary Sequence," *Astrophys. J.* **598**, pp. 1079–1099, Dec. 2003.
24. C. Aspin, G. Sandell, and D. A. Weintraub, "The remarkable pre-main sequence object V1318 Cygni," *Astron. Astrophys.* **282**, pp. L25–L28, Feb. 1994.
25. R. I. Davies, M. Tecza, L. W. Looney, F. Eisenhauer, L. E. Tacconi-Garman, N. Thatte, T. Ott, S. Rabien, S. Hippler, and M. Kasper, "Adaptive Optics Integral Field Spectroscopy of the Young Stellar Objects in LKHα 225," *Astrophys. J.* **552**, pp. 692–698, May 2001.
26. R. B. Larson, "Formation of star clusters," in *ASSL Vol. 162: Physical Processes in Fragmentation and Star Formation*, pp. 389–399, 1990.
27. E. C. Ostriker, "Capture and induced disk accretion in young star encounters," *Astrophys. J.* **424**, pp. 292–318, Mar. 1994.
28. H. M. J. Boffin, S. J. Watkins, A. S. Bhattal, N. Francis, and A. P. Whitworth, "Numerical simulations of protostellar encounters - I. Star-disc encounters," *Mon. Not. R. Astron. Soc.* **300**, pp. 1189–1204, Nov. 1998.
29. D. E. Potter and S. M. Andrews, "SR 24 N/S: A Case Study for Tidally Interacting CTTS Disks?," *Bulletin of the American Astronomical Society* **34**, pp. 1217–+, Dec. 2002.
30. M. Cohen and L. V. Kuhi, "Observational studies of pre-main-sequence evolution," ApJS **41**, pp. 743–843, Dec. 1979.
31. P. S. The, D. de Winter, and M. R. Perez, "A new catalogue of members and candidate members of the Herbig Ae/Be (HAEBE) stellar group," A&AS **104**, pp. 315–339, Apr. 1994.
32. A. Mora, B. Merín, E. Solano, B. Montesinos, D. de Winter, C. Eiroa, R. Ferlet, C. A. Grady, J. K. Davies, L. F. Miranda, R. D. Oudmaijer, J. Palacios, A. Quirrenbach, A. W. Harris, H. Rauer, A. Cameron, H. J. Deeg, F. Garzón, A. Penny, J. Schneider, Y. Tsapras, and P. R. Wesselius, "EXPORT: Spectral classification and projected rotational velocities of Vega-type and pre-main sequence stars," A&A **378**, pp. 116–131, Oct. 2001.
33. T. Henning, A. Burkert, R. Launhardt, C. Leinert, and B. Stecklum, "Infrared imaging and millimetre continuum mapping of Herbig Ae/Be and FU Orionis stars," *Astron. Astrophys.* **336**, pp. 565–586, Aug. 1998.
34. S. C. Casey and D. A. Harper, "VY Monocerotis and the IC 446 region - Far-infrared and submillimeter images of a massive young stellar object and its environment," ApJ **362**, pp. 663–673, Oct. 1990.
35. E. Habart, L. Testi, A. Natta, and L. Vanzi, "Mid-IR observations of small stellar clusters surrounding Herbig AeBe stars," A&A **400**, pp. 575–583, Mar. 2003.
36. B. R. Oppenheimer, A. P. Digby, L. Newburgh, D. Brenner, M. Shara, J. Mey, C. Mandeville, A. Sivaramakrishnan, R. B. Makidon, R. Soummer, J. R. Graham, P. Kalas, M. D. Perrin, L. C. Roberts, J. Kuhn, K. Whitman, and J. P. Lloyd, "The Lyot Project: Toward Exoplanet Imaging and Spectroscopy," in *This volume*, 2004.